Three-dimensional analysis of local scouring induced by a rotating ship propeller

Nadia Penna[a1], Felice D'Alessandro[a], Roberto Gaudio[b] and Giuseppe R. Tomasicchio[a]

[a]*Dipartimento di Ingegneria dell'Innovazione, Università del Salento, 73100 Lecce (LE), Italy (nadia.penna@unisalento.it)*

[b]*Dipartimento di Ingegneria Civile, Università della Calabria, 87036 Rende (CS), Italy*

Abstract

The jet induced by a rotating ship propeller can cause scouring of the seabed and consequent deposition of the scoured material nearby. Despite these effects are extremely important for the operability of a harbour, there is currently limited work concerning a detailed investigation of the three-dimensional (3D) characteristics of the bed topography changes induced by the ship propeller. Thus, this paper presents laboratory experiments with the aim of analysing the effects induced by a propeller on a mobile bed, in different conditions of submergence depth (h_0) and rotational speed (n). The equilibrium bed surface topography was acquired with the photogrammetry technique combined with a 3D Terrestrial Laser Scanner (TLS), in order to analyse, for the first time, bed elevation data obtained from high-resolution Digital Elevation Models (DEMs). As a result, it was demonstrated that the swirling jet produced by a rotating propeller causes the development of a bed topography not symmetrical with respect to the propeller longitudinal axis, with a deeper scour hole on one side and a higher deposition mound on the other side. Therefore, the scour hole induced by a propeller cannot be assimilated to that produced by a water jet and this behaviour can be noted only with a comprehensive and detailed analysis of a 3D model of the bed topography. Furthermore, it was shown that increasing n for the same h_0 (or reducing h_0 by keeping n constant) causes a longer, deeper and wider scour hole and a higher deposition mound, with a greater volume of sediments

[1] Present address: *Dipartimento di Ingegneria Civile, Università della Calabria, 87036 Rende (CS), Italy,* nadia.penna@unical.it.

eroded from the bed and deposited nearby the scour hole. To be precise, this is the first study aiming at estimating the eroded and deposited sediment volumes by a propeller jet, thanks to the use of the high-resolution DEMs. The relationships between all the involved variables were analysed, providing equations, graphs and an abacus for the prediction of the effects induced by the propeller as a function of h_0 and the Froude number.

Keywords Propeller scour, Unconfined scouring, Photogrammetry technique, Sediment transport.

1. Introduction

The traditional marine propulsion system used to move a ship is constituted by an electric motor turning a propeller (sometimes two propellers), generally manufactured with more than three blades. The device produces a turbulent jet that impacts the seabed and banks of harbour basins or navigation channels up to a distance of several propeller diameters from them (Hamill, 1999). As outlined by many authors, the ship propeller jet can cause two main effects: scouring and deposition of scoured material. Specifically, Hong et al. (2013) stated that the resulting bed topography profile along the jet centreline consists of three parts: a small scour hole beneath the propeller, a primary (main) scour hole downstream of the propeller and a deposition mound. The scouring phenomenon can affect the stability of quay structures, whereas deposition of sediments may cause a reduction of the average water depth (e.g., Whitehouse, 1998; Abramowicz-Gerigk, 2010; Lam et al., 2011; PIANC, 2015; Mujal-Colilles et al., 2017; Yew et al., 2017; Wei and Chiew, 2018). Froehlich and Shea (2000) have shown that essential cover to buried pipelines, tunnels and contained aquatic disposal sites can also be removed by propeller induced flows. Other important effects of the propeller jet on the environment are the resuspension of fine sediments and the injection/dispersion into the water of oil and fuel released from large vessels (Kelly et al., 2005; Ji et al., 2014; Hong et al., 2015), which negatively affect the benthic fauna in the aquatic environment and the ecological system (Hamill et al., 2015). All these problems and damages become more significant if continued mooring and unmooring of ships occur always at the same position (e.g., Sumer and Fredsøe, 2002; Qurrain, 1994; Hamill et al., 2015) and when the ships are loaded and the tide is at its lowest. For all these reasons, the investigation of the effects of the ship propeller jet have received continuous worldwide attention by civil, maritime/hydraulic and naval engineers, in order to understand the mechanism of bed scouring, to propose possible countermeasures and, therefore, to limit the operating costs for the necessary repair works.

In the light of above, the aim of the present study is to investigate experimentally the characteristic dimensions of the scour hole (such as scour depth, d_s, scour length, l_s, scour width, b_s) induced by the rotation of a ship propeller, together with the height of the deposit mound, h_d, in the neighbourhood of the scour hole and the eroded and deposited volumes, V_e and V_d, respectively, at the end of the scouring phase. Toward this end, a highly detailed 3D topographical analysis was carried out by using the photogrammetry technique combined with a 3D Terrestrial Laser Scanner (TLS). Monitoring of such quantities is extremely important as several harbours worldwide face the problem of hosting ships with higher depths and engine powers than those for which they were designed (e.g., Berg and Magnusson, 1987; Schokking et al., 2003), thus decreasing their efficiency and operability with consequent significant economic losses (Mujal-Colilles et al., 2017, Smith et al., 2017).

The paper is structured as follows: in the next section, a state-of-the-art review of the most important laboratory experimental research on propeller jet is presented. The experimental setup and the methodology used in this study follow. Also the description of the procedures adopted for the acquisition of bed surface data (by using the photogrammetry technique and the TLS) and then for the post-processing of the data are furnished. Thus, a brief review of the methods applied for the statistical analyses is given. In the section "Results and discussion", the results are critically analysed and discussed comparing the experimental tests and highlighting the agreements and disagreements of the present findings with the literature ones. In the final section, "Summary and conclusions", the results of this study are summarised along with concluding remarks.

2. State of the art

The earliest investigations on this topic were focused on the velocity characteristics within a ship propeller jet using the axial momentum theory and a plain water jet, as it was documented by Ozan and Yüksel (2010), Yeh et al. (2009) and Yüksel et al. (2005). Actually, the velocity characteristics of a ship propeller jet are more complicated than those of a plain water jet (Lam et al., 2012) and, therefore, also the resulting scour holes are far different. Several researchers focused their work on the prediction of the maximum scour depth in the absence of berthing structures (e.g., Blaauw and van de Kaa, 1978; Hamill, 1987; Hong et al., 2013; Tan and Yüksel, 2018), considering the efflux velocity as the main driving force for scouring. Stewart (1992), Hashmi (1993), Qurrain (1994), Hamill et al. (1999) and Ryan (2002) extended the studies by including the effect of propellers on perpendicular and/or parallel quay walls. More recently, the case of the propeller scour in presence of an open type quay has received great attention. For example, Yüksel et al. (2018) studied the scouring mechanism due to propeller jet flow for an open-type berth structure with the presence of a single pile. Wei and Chiew (2017) analysed the influence of toe clearance on the scour formation; later, Wei and Chiew (2018) performed velocity measurements for the characterization of the propeller jet flow using a Particle Image Velocimetry (PIV) system. Ozan et al. (2012) investigated the effect of propeller jet flow on the stability of an armoured slope under berth structures. Finally, both Cihan et al. (2012) and Wei et al. (2018) studied the propeller scour around a sloping bank.

However, there is currently limited work concerning a detailed investigation of the three-dimensional (3D) characteristics of the scour hole induced by a ship propeller jet in both unconfined and confined situations. To be more specific, the *confined condition* occurs when the jet is confined by a vertical wall, otherwise the *unconfined condition* takes place. Only Wei and Chiew (2017) measured the 3D topography of the scour hole using an Acoustic Doppler Velocimeter (ADV) over a 20 mm x 20 mm grid, demonstrating that the scour profiles in the vicinity of toe clearance at the asymptotic state were highly asymmetrical. The degree of asymmetry diminishes increasing the toe clearance, corroborating the hypothesis of Hamill (1987): the scour profile induced by an unconfined propeller jet is symmetrical along the jet centreline.

Thus, under different experimental conditions, such as submergence depth and rotational speed, the aims of the proposed research are: (1) to provide insight on the scouring and deposition phenomena due to the overlapping effects of more than one ship until reaching the equilibrium scour condition; (2) verify the symmetry hypothesis of Hamill (1987) in unconfined propeller situation.

3. Methods

3.1. Experimental setup

The experimental tests were performed in an 18 m long, 0.985 m wide and 0.7 m deep horizontal flume with rectangular cross-section at the *Laboratorio "Grandi Modelli Idraulici"*, *Università della Calabria*, Italy. A 2.5 m long, 0.985 m wide and 0.30 m deep recess box is installed at 11.5 m downstream of the inlet, in correspondence of lateral glass observation windows that are mounted on both sides. All the tests were performed in still water condition with a water depth h = 0.25 m. The sediment recess box was filled in with sediments having median diameter d_{50} = 0.69 mm, geometric standard deviation $\sigma_g = \sqrt{d_{84}/d_{16}}$ = 1.4 and specific sediment weight γ_s = 2660 kg/m^3. The propulsion system was constituted of an electric motor turning a propeller with four blades, having diameter D_p = 8.2 cm. Both D_p and d_{50} were set in accordance to literature datasets (e.g., Hamill, 1987; Tan and Yüksel, 2018), which constitute a reference framework for our results. Additionally, the ratio h/D_p respects literature values (e.g., Hamill, 1987; Hong et al., 2013), indicating that its effect can be neglected as the water level is large enough with respect to D_p. The propeller characteristics are listed in Table 1. All the quantities shown in Table 1 were directly measured, except for the Expandend Area Ratio (EAR) and the thrust coefficient C_t. Specifically, the EAR was calculated as the ratio between the Total Blade Area (TBA) and the Propeller Disc

Area (PDA). The TBA is defined as bA_b, where b is the number of blades and A_b is the area of each blade, whereas the PDA is the area of a disc having a diameter equals to that of the propeller. As regards C_t, it varies with the propeller type. Specifically, C_t was determined considering literature data referring to a propeller with similar diameter (e.g. Hamill et al., 2015; Lam et al., 2010; Qurrain, 1994), which usually ranges from 0.3 to 0.4. An inverter electronic circuit controls the motor, with a low voltage of maximum 24 V. To avoid the overheating of the motor during the experimental tests, a water cooling system is installed around it. The motor can operate up to 1600 revolutions per minute (rpm). A speedometer was used to set the desired rotational velocity. During the experiments, the whole propulsion system was firmly attached to a frame in the middle of the channel and at the beginning of the recess box, preventing its movement around the vertical and transverse axes. Figure 1 illustrates the experimental apparatus used in the present study, whereas the hypothetical longitudinal profile of the scour hole formed by a rotating ship propeller is shown in Figure 2.

Table 1 - Characteristics of the propeller used in the study.

Propeller characteristics	
Propeller diameter, D_p (cm)	8.20
Hub diameter, D_h (cm)	1.20
Blade number, b	4
Expanded Area Ratio (EAR) without hub, β	0.52
Thrust coefficient, C_t	0.40

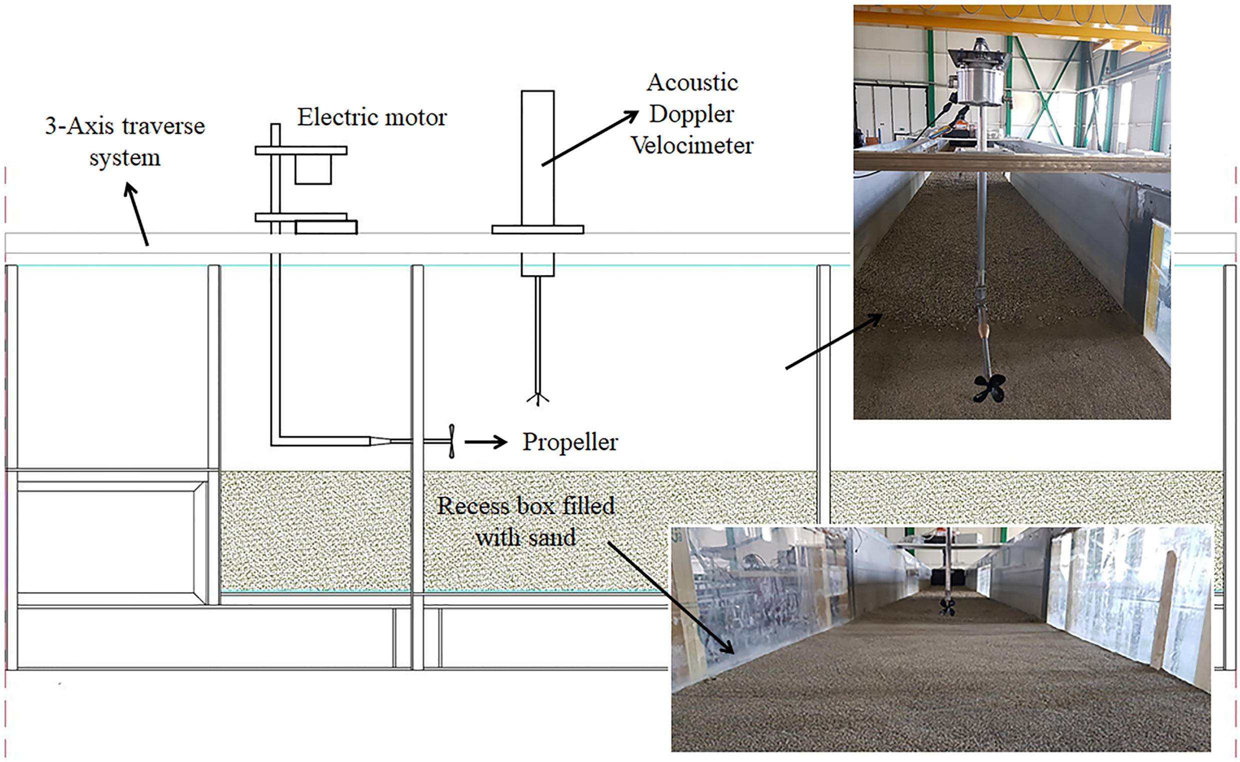

Figure 1 - Experimental apparatus used in the present study at the *Laboratorio "Grandi Modelli Idraulici"*, *Università della Calabria*.

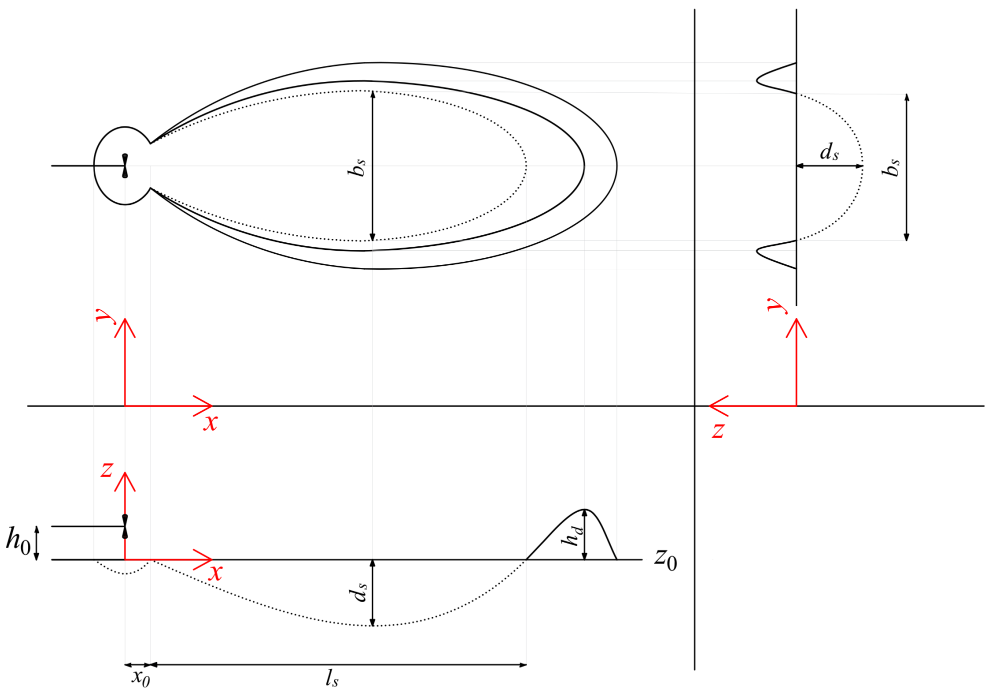

Figure 2 - Hypothetical scour hole formed by a rotating ship propeller, b_s being the maximum scour width, d_s the maximum scour depth, l_s the maximum scour length, h_d the maximum deposit height, h_0 the submergence depth of the propeller and z_0 the initial bed surface level.

Specifically, three different rotational speed (n) in anticlockwise direction were tested, considering three submergence depths (h_0), defined as the distance between the propeller hub and the bed surface before the start of the test. These hydraulic and geometric conditions were chosen to simulate three different draughts of the ship having low, intermediate and high rotational speeds, whose values were set in accordance to literature tests (e.g., Wei and Chiew, 2017; Tan and Yüksel, 2018). Table 2 shows a summary of the experimental conditions of the tests conducted in this study. In particular, the efflux velocity U_0 was calculated using the equation (1) proposed by Hamill et al. (2015), which is used in some current design guidelines (Wei and Chiew, 2017):

$$U_0 = 1.22 n^{1.01} D_p^{0.84} C_t^{0.62}, \tag{1}$$

where n is expressed in revolution per seconds (rps). The formula was tested for four propellers of D_p = 7.6 cm, 9.2 cm, 10.3 cm and 13.1 cm with $0.4 < C_t < 0.56$ for $0.4 < \mathrm{EAR} < 0.922$. These characteristics are similar to those of the propeller used in this study. The propeller Reynolds number Re_p is expressed by equation (2):

$$Re_p = \frac{n D_p L_m}{\nu}, \tag{2}$$

where L_m is the characteristic length and ν is the kinematic viscosity of the fluid (10^{-6} m^2·s^{-1} at a temperature of 20 °C). The L_m term was defined by Blaauw and van de Kaa (1978) and is dependent on the EAR without hub β, N, hub diameter (D_h) and D_p, as reported in equation (3):

$$L_m = \beta D_p \pi \left[2N \left(1 - \frac{D_h}{D_p} \right) \right]^{-1}. \tag{3}$$

Verhey (1983) suggested that the scaling effects due to viscosity can be avoided if the jet Reynolds number Re_f and the propeller Reynolds number Re_p are greater than $3 \cdot 10^3$ and $7 \cdot 10^4$, respectively. In the present study, the Re_p values are lower than the limiting value. However, Blaauw and van de Kaa (1978) and Verhey (1983) stated that the scale effects attributable to the noncompliance of the viscous effects are likely not significant. This hypothesis was later confirmed by Lam et al. (2010) and Hamill and Knee (2016).

Table 2 – Summary of the experimental conditions for each test, where t is the total test duration, U_0 the efflux velocity, $F_0 = U_0/(gd_{50}\Delta)^{0.5}$ the densimetric Froude number, Δ the relative submerged grain density, $Re_f = U_0D_p/\nu$ the jet Reynolds number and Re_p the propeller Reynolds number.

Test	h_0 (m)	t (h)	n (rpm)	U_0 (m·s^{-1})	F_0	Re_f	Re_p
A1	0.082	120	270	0.39	3.65	$3.17 \cdot 10^4$	$7.24 \cdot 10^3$
A2	0.082	139	480	0.69	6.52	$5.66 \cdot 10^4$	$1.29 \cdot 10^4$
A3	0.082	120	700	1.01	9.54	$8.29 \cdot 10^4$	$1.88 \cdot 10^4$
B1	0.068	98	270	0.39	3.65	$3.17 \cdot 10^4$	$7.24 \cdot 10^3$
B2	0.068	144	480	0.69	6.52	$5.66 \cdot 10^4$	$1.29 \cdot 10^4$
B3	0.068	150	700	1.01	9.54	$8.29 \cdot 10^4$	$1.88 \cdot 10^4$
C1	0.096	110	270	0.39	3.65	$3.17 \cdot 10^4$	$7.24 \cdot 10^3$
C2	0.096	165	480	0.69	6.52	$5.66 \cdot 10^4$	$1.29 \cdot 10^4$
C3	0.096	162	700	1.01	9.54	$8.29 \cdot 10^4$	$1.88 \cdot 10^4$

3.2. Experimental tests

A four-beam down-looking acoustic Doppler velocimeter (ADV) probe (Nortek Vectrino) was used to measure the initial bed level as a reference elevation at the centreline with a space resolution of 2 cm.

Similarly, the development of the scour along the centreline was monitored with time to estimate the achievement of the equilibrium scour condition. Beyond the equilibrium time (t_e), the bed topography remains unchanged. During each test the measurements were performed without switching the propeller off, in order not to affect the overall scouring formation, using a motorized 3-axis traverse system (HR Wallingford) on top, allowing an easy movement of the ADV probe during the experimental test with a constant velocity equals to 50 mm/s. Therefore, the time required for the measurement of each profile depended on the scour and deposit lengths to be acquired. The longest profile measured was about 1.3 m (Test A3) and it was acquired in less than 1 minute.

At the end of the scour process, the flume was slowly emptied without any disturbance for the bed topography by using two bottom outlets located 3 m upstream to and 2.3 m downstream of the test section, respectively. Hence, the 3D bed surface topography was acquired with the photogrammetry technique. Specifically, for each experimental test, about 110 photographs were taken with a Nikon D5200 camera, equipped with the Nikkor 18-55mm f/3.5-5.6G VR lens, from the left and right walls of the flume, covering a distance of about 2.5 m. The camera positions were oriented downwards at an oblique angle of about 45°. The photographs were aligned by using the software *PhotoScan* (Agisoft), considering 36 different targets placed on the flume walls. The software allowed the creation of a 3D point cloud and, subsequently, of an unstructured triangular mesh. Owing to the high number of photographs used in this study, no holes were detected in the point clouds of all the experimental tests.

Then, the flume was scanned by using the TLS (Leica ScanStation P20) from three separate stations, one at the upstream end of the recess box, one at the downstream end of it and one lateral to the scour hole. The resolution of the TLS data acquisition was set in order to obtain a vertical and horizontal spacing of 1 cm at a distance of 10 m from the instrument. The data derived from the TLS were processed using the manufacturer's software, *Cyclone 9.0* (Leica Geosystems) for the alignment of the three separate stations and the creation of a "reference point cloud". This latter was used for the scaling of the 3D surface resultant from the photogrammetry technique.

Hence, once the unstructured triangular mesh was scaled, for each experimental test, the structured grid was extracted using the commercial software *Rhinoceros* (McNeel & Associates), with a spatial resolution δl = 5 mm in both the streamwise and spanwise directions. The consistency between the measurements performed with the ADV and those derived by the 3D modelling was evaluated for each experimental test. Finally, an algorithm was implemented in a *Matlab* (MathWorks) code, programmed on purpose, and thus applied to the bed elevation data, in order to statistically analyse the grid, to determine the characteristic dimensions of the scour hole and of the deposit (longitudinal and transversal profiles, $d_{s,\max}$, $l_{s,\max}$, $b_{s,\max}$, $h_{d,\max}$) and to calculate V_e and V_d.

3.3. Statistical analysis of the bed elevation data

The right-handed Cartesian coordinate system convention was adopted in this study, where the origin of the *x*-axis (streamwise direction) is set in correspondence of the propeller, whereas the *y*-axis and the *z*-axis indicate the spanwise and the vertical direction, respectively.

The final bed elevation at the i-th location was defined as $z_i = z_0 - z_i'$, where z_i' is the bed elevation at i-th location measured on the 3D model, z_0 is the initial mean bed elevation derived from the ADV measurements before starting the experiment and z_i is the fluctuation of z_i' with respect to z_0.

Initially, having removed the respective z_0 value from the bed elevation data, the structured grids for all the bed configurations were used to estimate the probability density functions (PDFs) and their properties, such as the standard deviation σ_z, the skewness Sk_z and the kurtosis Ku_z, defined by equations (4-6):

$$\sigma_z = \sqrt{\frac{1}{NM-1}\sum_{i=1}^{NM} z_i'^2}, \quad (4)$$

$$Sk_z = \frac{1}{NM\sigma_z^3}\sum_{i=1}^{NM} z_i'^3, \quad (5)$$

$$Ku_z = \frac{1}{NM\sigma_z^4}\sum_{i=1}^{NM} z_i'^4, \quad (6)$$

where $i = 1, 2, 3, \cdots, N\times M$, assuming that N and M are the grid points in streamwise and spanwise direction, respectively. Specifically, σ_z can be interpreted as an estimate of the statistical dispersion of the data, Sk_z signifies a measure of the asymmetry of the data about the mean value and Ku_z is a measure to define how outlier-prone a PDF is. If the bed elevation field is stationary, homogeneous and Gaussian, then Sk_z and Ku_z should be equal to 0 and 3, respectively. In this case, the existence of a plane of symmetry is expected with respect to the scour hole formed by the rotating propeller.

4. Results and discussion

4.1. Scour formation

In all the tests the scour formation was observed. Figure 3a shows the critical curve for the scour initiation under the propeller jet mechanism proposed by Hong et al. (2013). The left-hand side of the lines represents no scour conditions, whereas the right-hand side of them corresponds to scouring formation. It is readily noticeable that the results of the present study are in agreement with the critical curve revised by Tan and Yüksel (2018), who considered in their experiments a wider range of both h_0/D_p and F_0 with respect to Hong et al. (2013).

As an example, Figure 4 shows the plan view of the 3D models of the bed surface topography for the experimental tests A1 to A3 obtained at the equilibrium stage using the photogrammetry technique. The effect produced by the propeller consists in a small scour hole directly beneath the propeller and a main scour hole that expands downstream of it, also along the y-axis, and creates a sediment mound that moves downwards and enlarges gradually. The extension of these regions depends on F_0, i.e., on n; in fact, for the lowest rotational speed the small scour does not appear, whereas increasing n both the scour holes become wider and longer. This is in accordance to the findings of Tan and Yüksel (2018), who proposed a functional relationship between h_0/D_p and F_0 to determine the small scour formation (Fig. 3b).

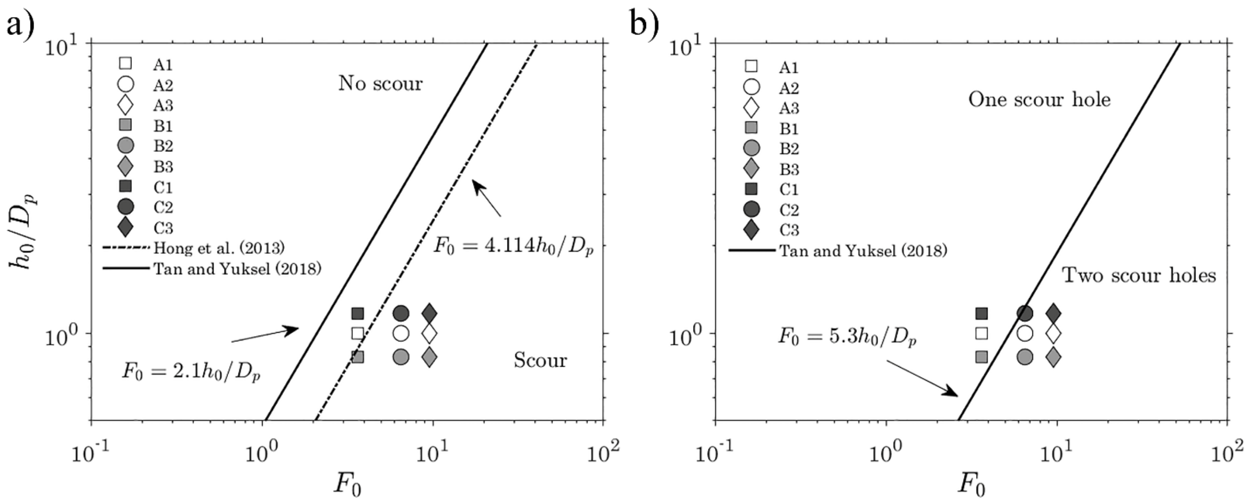

Figure 3 - a) Critical curves for the initiation of scouring and b) scour formation curve for one or scour holes proposed by Tan and Yuksel (2018).

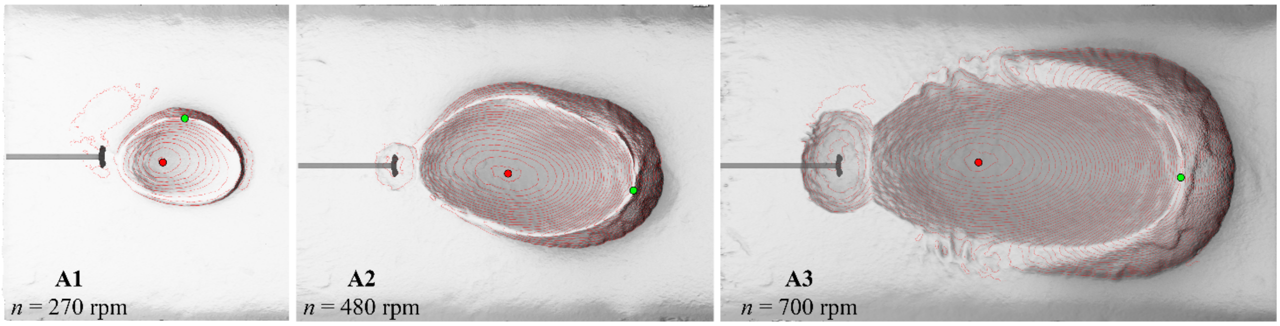

Figure 4 - Plan view of the 3D models and contours of the bed surface topography for tests A1 to A3. The red and green points indicate the position where d_s and h_d occur, respectively.

Figures 5 (a-d-g) illustrate the evolution of the longitudinal bed profile at the centreline for tests C1 to C3, from the initiation of the scouring process until reaching the equilibrium condition. For test C1 a particular configuration was observed: two deposition mounds were created immediately upstream to and downstream of the main scour hole, indicating that the zone below the propeller is not affected by its presence and that the trajectory of the jet impacts the bed at a distance of about 10 cm from the propeller. Note that test C1 is characterized by the highest value of submergence depth (h_0 = 0.096 m) and lowest rotational speed (n = 270 rpm).

The data analysis reveals that, in the equilibrium phase, the maximum scour depth at the centreline (d_{sc}) is not always the maximum value reached during the scouring process (see Fig. 5d). Initially, the bed tends to be eroded in the streamwise direction, shifting the location of the maximum scour depth downstream. Owing to the eroded sediments coming from upstream, a deposition phenomenon occurs in the scour hole, temporarily decreasing the maximum scour depth. Once the equilibrium phase is achieved in the upstream part of the scour hole, it progressively increases its depth. The behaviour is well described in Figs. 5 (b, e, h), in which the scour rates in terms of maximum depth ($\Delta d_{sc}/\Delta t$) and length ($\Delta l_{sc}/\Delta t$) along the centreline (measured starting from the abscissa x_0 corresponding to the beginning of the main scour hole) were plotted: at first, $\Delta l_{sc}/\Delta t$ is much higher than $\Delta d_{sc}/\Delta t$ and then they both rapidly decrease, reaching the equilibrium condition (when their values are next to 0 and the dimensions of the scour hole remain unchanged over time).

In order to verify that the profiles exhibit a similar behaviour over time, their vertical and horizontal dimensions were normalized with d_{sc} and l_{sc}, respectively (determined at the equilibrium condition along the centreline). The data in the respective Figs. 5 (c, f, i) show that the scour hole profiles are affine, since the normalized scour profiles generally fall inside a narrow band. The maximum scour depth occurs at $(x - x_0)/l_{sc}$ = 0.30 to 0.60. However, at the initial scouring phase the data exhibits the greatest scatter, as it was observed by Hong et al. (2013) in their experiments, deducing that the scouring rate is more uncertain at the early stage of the scouring process. With time, the scouring rates decrease and the profiles collapse. It is possible to note that the affinity is also preserved for the deposition mound in the last phase of scouring.

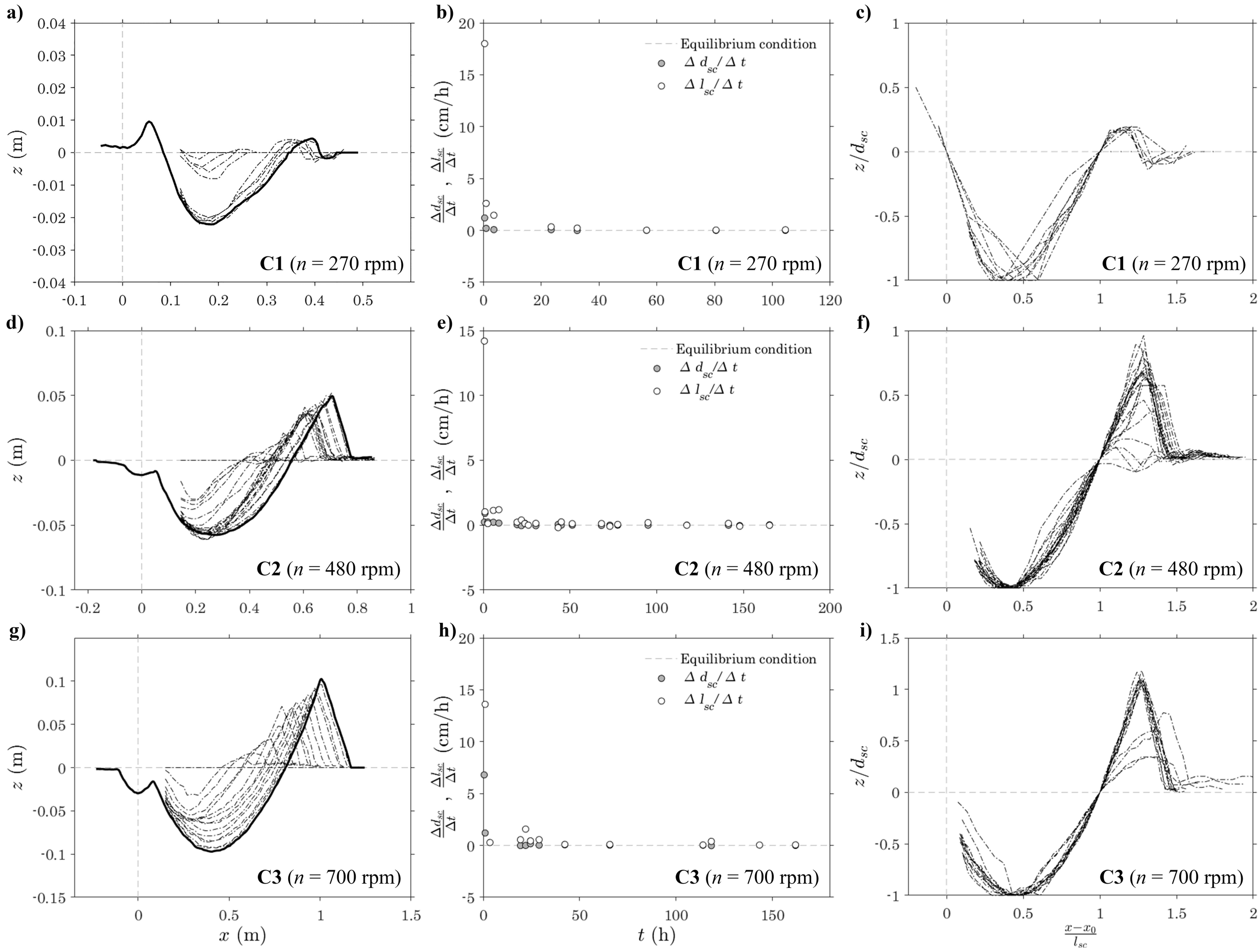

Figure 5 – Tests C1 to C3: (a, d, g) temporal development of the centreline profile; (b, e, h) rate of scour in terms of maximum depth and maximum length; (c, f, i) nondimensional scour profiles.

4.2. Centreline longitudinal bed profiles at the equilibrium condition

Figure 6 shows the centreline longitudinal bed profiles at equilibrium for all the tests. Data clearly highlights how the rotational speed and, to a less extent, the submergence depth influence the scour profile. Increasing *n* for the same h_0 causes a longer and deeper scour hole and a higher deposition mound (see, e.g., tests A1 to A3). This means that the propeller jet tends to expand downstream and in depth, with vortexes more elongated in the streamwise direction with respect to the spanwise direction. The same occurs, but with minor evident effects, if h_0 is reduced by keeping a constant rotational speed (see, e.g., the comparison between tests A1 to A3 and C1 to C3, respectively).

However, for tests B1 to B3, characterized by the lowest value of h_0, a different behaviour was discovered: increasing the rotational speed, a deeper scour hole and a higher deposition mound were formed; nevertheless, the scour holes are shorter if compared to those of test A1 to A3, respectively. Hence, it may be inferred that, when the propeller is close to the bed surface, the induced vortex system tends to expand in depth and to a lesser extent downstream. At the same time, the deep scour thus formed may prevent further elongation of the scour hole and the entrained sediment particles from being transported downstream.

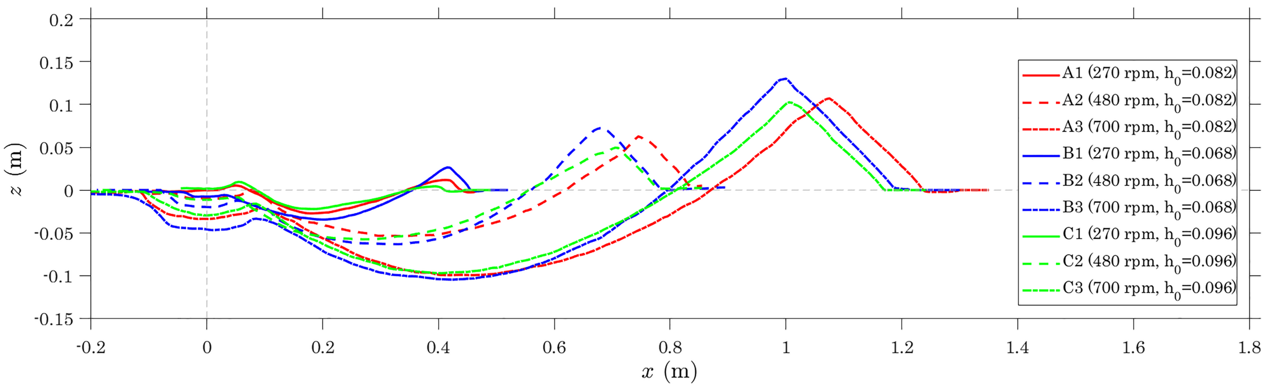

Figure 6 - Centreline longitudinal bed profiles at equilibrium.

Table 3 shows for each test the values of the maximum scour length, maximum scour depth and maximum deposit height, obtained from the analysis of the centreline longitudinal bed profiles at equilibrium (l_{sc}, d_{sc} and h_{dc}, respectively).

In Fig. 7 the relationship between F_0 and the dimensionless scour length at the centreline (l_{sc}/D_p) is shown. Specifically, the data were compared to the equations proposed by Tan and Yüksel (2018), valid for a propeller jet, and by Chiew and Lim (1996), valid for a circular water jet from a wall. Note that for the water jet formula the diameter of the circular jet D_0 was assumed equal to D_p. It is evident that, although the data tends to follow the propeller jet formula, this latter is slightly shifted upward. Hence, the propeller jet formula was modified as reported in equation (7):

$$\frac{l_{sc}}{D_p} = F_0 \tag{7}$$

obtaining a coefficient of determination R^2 equal to 0.96. This means that F_0 alone can be used to easily estimate the maximum scour length along the centreline. The slope of the lines valid for the propeller jets are different, leading to a longer scour hole for the data of the present study with respect to the results obtained by Tan and Yüksel (2018) considering the same F_0. The new proposed formula was also validated with the experimental data of Hamill (1987), giving more than satisfactory results, as observed in Fig. 7. It is also noticeable that the circular wall jet formula cannot be used to predict the length of the scour hole, implying that the scour hole induced by a propeller cannot be assimilated to that produced by a water jet.

Table 3 – Measured characteristics of the scour hole.

Test	l_{sc} (cm)	d_{sc} (cm)	h_{dc} (cm)	d_s (cm)	h_d (cm)	b_s (cm)	V_e (m^3)	V_d (m^3)	ε (%)
A1	27.3	2.72	1.17	2.75	2.48	18.0	$8.02\cdot10^{-4}$	$7.49\cdot10^{-4}$	6.70
A2	54.0	5.39	6.27	5.58	6.39	33.0	$5.00\cdot10^{-3}$	$4.90\cdot10^{-3}$	0.43
A3	77.5	9.96	10.71	10.00	11.25	54.5	$1.66\cdot10^{-2}$	$1.63\cdot10^{-2}$	1.57
B1	32.5	3.46	2.64	3.46	3.50	23.5	$1.30\cdot10^{-3}$	$1.20\cdot10^{-3}$	3.81
B2	50.8	6.33	7.24	6.76	7.67	36.3	$5.40\cdot10^{-3}$	$5.20\cdot10^{-3}$	4.53
B3	71.0	10.48	13.02	10.56	13.20	55.0	$1.75\cdot10^{-2}$	$1.72\cdot10^{-2}$	1.81
C1	26.1	2.21	0.96	2.24	2.03	18.0	$7.53\cdot10^{-4}$	$7.38\cdot10^{-4}$	1.96
C2	50.5	5.76	4.95	5.81	5.27	33.0	$4.90\cdot10^{-3}$	$4.90\cdot10^{-3}$	1.42
C3	72.5	9.72	10.26	9.76	10.31	49.5	$1.44\cdot10^{-2}$	$1.42\cdot10^{-2}$	1.70

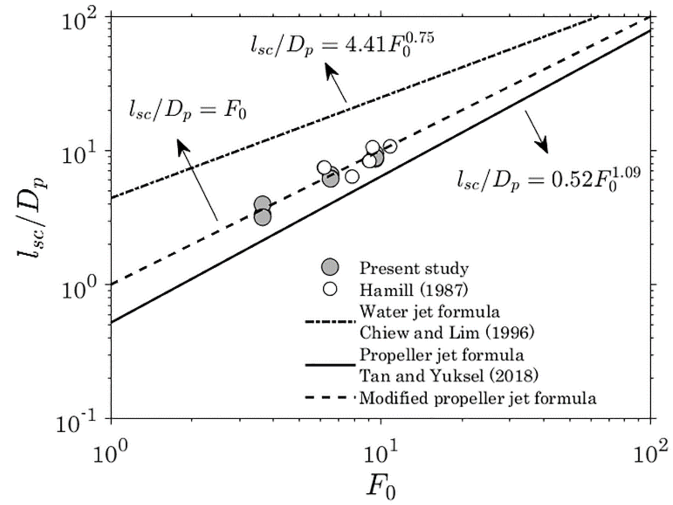

Figure 7 - Relationship between F_0 and l_{sc}/D_p.

The relationship between F_0 and the dimensionless scour depth at the centreline (d_{sc}/D_p) is illustrated in Fig. 8. As observed by Tan and Yüksel (2018), the equation proposed by Chiew and Lim (1996) for the water jet does not fit the experimental data of Hamill (1987) nor of the present study. This is due to the fact that a water jet causes more effective erosion than a propeller jet at the same efflux velocity, owing to the incidence angle of the jet with respect to the bed (Hawkswood et al., 2013). On the contrary, there is a good agreement with the trend proposed by Tan and Yüksel (2018), albeit with greater differences compared to the case of l_{sc}. The reason behind this fact is explained in the next section.

Finally, in order to characterize the development of the deposition mound as a function of the rotational speed of the propeller, a relationship is proposed [equation (8)] to link the dimensionless deposit height at the centreline h_{dc}/D_p with F_0 (Fig. 9), defined as:

$$\frac{h_{dc}}{D_p} = 0.024F_0^{1.80} \tag{8}$$

with a coefficient of determination R^2 equal to 0.93. However, the estimation of h_{dc} using the proposed formula may be affected by not negligible errors especially for low F_0, for which the deposit height could be overestimated. The reason behind this fact is explained in the next section.

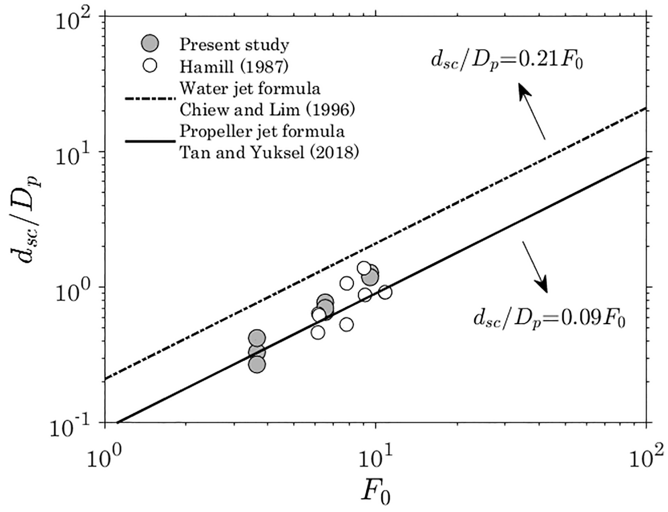

Figure 8 - Relationship between F_0 and d_{sc}/D_p.

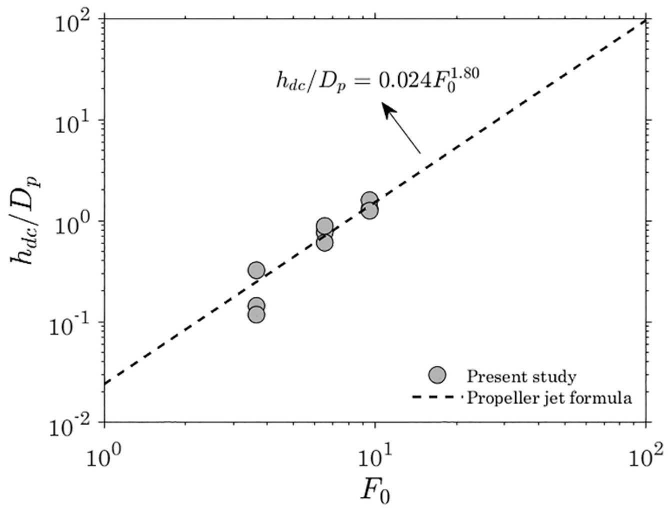

Figure 9 - Relationship between F_0 and h_{dc}/D_p.

4.3. 3D analysis of the scour hole

Figure 4 illustrates, as an example, the location of the maximum scour depth (d_s, indicated with a red circle) and the maximum deposit height (h_d, indicated with a green circle) determined over the whole 3D domain for tests A1 to A3. The corresponding values are shown in Tab. 3. For each configuration, although the minimum point is in proximity of the central region of the main scour hole, it is not exactly in correspondence of the propeller axis and, above all, the maximum is always decentralized with respect to it. This means that the general hypothesis that considers the scour hole symmetrical with respect to the centreline (in correspondence of the propeller) is not verified. This important finding contrasts with previous studies on unconfined propeller jets (e.g., Hamill, 1987; Hong et al., 2013; Tan and Yüksel, 2018), for which the scour hole is nearly symmetrical with respect to the propeller axis, with a slight asymmetrical deposition on its transverse sides. Actually, the scour resulted highly asymmetrical in all the performed experimental tests, especially for low and intermediate F_0 (tests A1-A2, B1-B2 and C1-C2). The explanation for this behaviour lies in the nature of the jet produced by the rotating propeller: it is essentially a swirling jet that causes the sediment particles to be detached from the movable bed and transported by the vortical structures, which, following the direction of the propeller rotation, are responsible of the development of the main scour hole. Thus, the maximum scour depth, as well as the maximum deposit height, does not necessarily occur at the centreline because of this swirling effect. Such a tendency was also found by Wei and Chiew (2017) for a confined propeller jet in the presence of an open type quay.

In particular, since in this study a left-hand propeller was used, a counterclockwise direction of rotation was obtained (looking upstream). Thus, it was expected that the scour hole was deeper on the left side of the propeller and the deposition mound was higher on its right side. Indeed, for the lowest rotational speed of the propeller, finer suspended particles tended to settle to the right side of the propeller, where a mound was formed. Increasing n, h_d had a tendency to move downwards and towards the right wall of the flume, where the effect induced by the propeller was dumped and the particles settled more easily, without any disturbance.

It is important to highlight that only with a comprehensive and detailed analysis of the 3D characteristics of the scour hole it is possible to capture such a particular phenomenon. In fact, in order to demonstrate numerically what was observed during the experimental measurements, the PDFs of bed elevations belonging to the right and left sides of the propeller were determined separately, together with the standard deviation σ_z, skewness Sk_z and kurtosis Ku_z. As an example, Fig. 12 shows the PDFs of the bed elevations of the right and left sides of the propeller (looking upstream) determined for tests B1 to B3. To make a comparison, the PDF of the right side was assumed to be positive and that of the left side negative. From the analysis of Fig. 10, it is readily noticeable that all the PDFs present a non-Gaussian distribution, characterised by $Sk_z \neq 0$ and $Ku_z \neq 3$. Furthermore, the left and right PDFs are always different (see σ_z), with a greater number of negative z-values (scour) at left of the propeller and a greater number of positive z-values (deposition) at right. This confirms that the scour hole is asymmetrical with respect to the propeller axis (that is the centreline) and that the scour is more pronounced on the left side of the propeller, since it depends on its rotation direction.

The swirling effect generated by the propeller causes the deviation of the experimental data concerning d_{sc} and h_{dc} from the respective predicting formulae (observed in Figs. 8 and 9), especially in the case of low F_0, for which the asymmetry was more evident. Therefore, two different new relationships are proposed [equations (9-10)] to link the dimensionless maximum scour depth (d_s/D_p) and maximum deposit height (h_d/D_p) to F_0 (see Figs. 11 and 12), as follows:

$$\frac{d_s}{D_p} = 0.06 F_0^{1.34} \tag{9}$$

$$\frac{h_d}{D_p} = 0.04 F_0^{1.53} \tag{10}$$

with a coefficient of determination R^2 equal to 0.98 and 0.93, respectively.

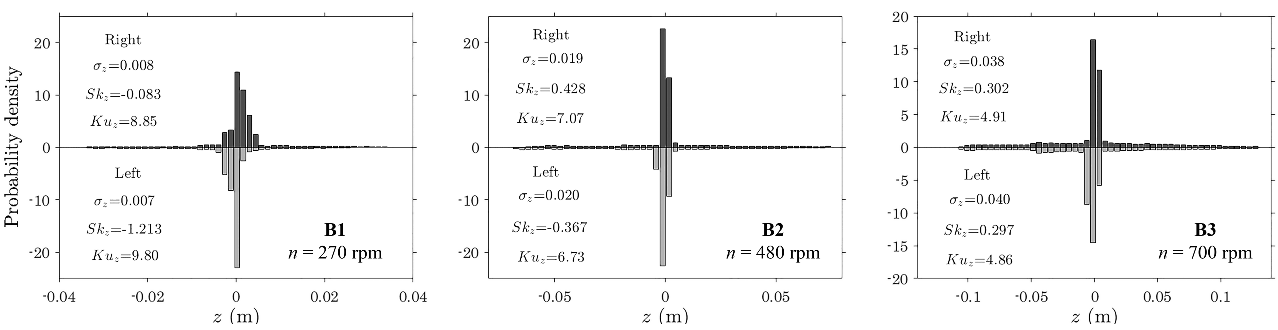

Figure 10 - PDFs of the bed elevations belonging to the right and left sides of the propeller (looking upstream) for tests B1 to B3.

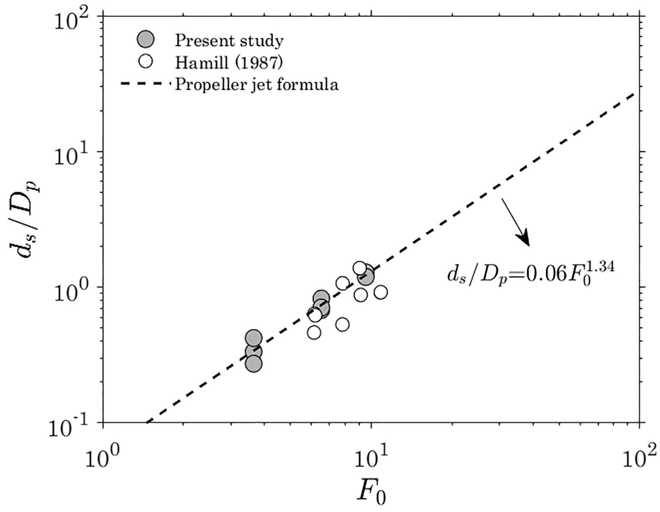

Figure 11 - Relationship between F_0 and d_s/D_p.

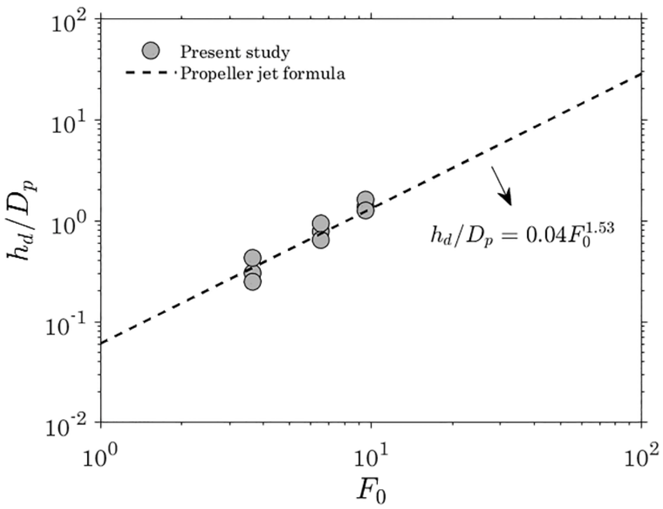

Figure 12 - Relationship between F_0 and h_d/D_p.

4.4. Transverse scour profiles at the maximum scour depth

Figure 13 depicts the transverse profiles measured at the location of the maximum scour depth and at equilibrium for all the tests. The data clearly highlights the asymmetry that characterises each profile from the centreline: a deeper scour hole on the left side of the propeller and a higher deposition mound on its right side. Moreover, it is possible to note how increasing n, for the same h_0, causes a deeper and wider scour hole (see, e.g., tests A1 to A3). The same occurs, but with minor evident effects, if h_0 is reduced keeping a constant rotational speed (see, e.g., the comparison between tests B1 to B3 and C1 to C3, respectively).

Table 3 shows for each test the values of the maximum scour width (b_s) obtained from the analysis of the transverse bed profiles at equilibrium. At the same time, Fig. 14 illustrates the relationship between F_0 and the dimensionless scour width (b_s/D_p). The data of the present study were compared with the equations proposed by Tan and Yüksel (2018) and by Chiew and Lim (1996). As observed, the data are well fitted by the propeller jet formula, which, therefore, does not require any further modification.

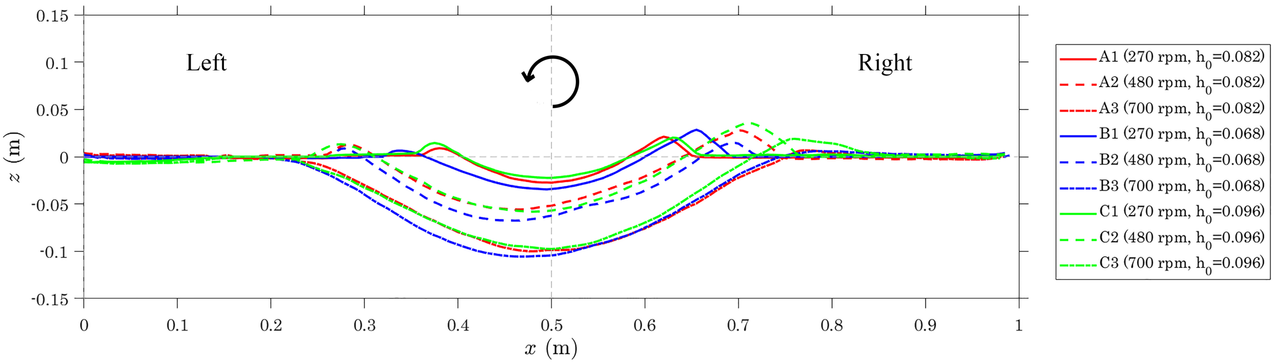

Figure 13 - Transverse bed profiles at the location of the maximum scour depth at equilibrium.

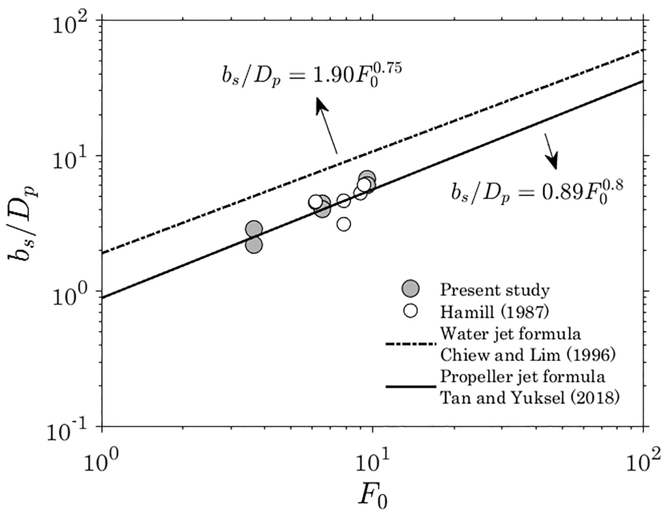

Figure 14 - Relationship between F_0 and b_s/D_p.

4.5. Assessment of the eroded and deposited sediment volumes

In this study, besides investigating the characteristic dimensions of the scour hole, the eroded and the deposited sediment volumes were determined, because of their great importance for possible dredging and filling works of the scour holes produced by ship propellers in a harbour.

On the basis of the dense data grids obtained with the 3D modelling of the bed surface of each experimental test, the V_e and V_d were determined for each calculation cell and their sums are reported in Tab. 3. As one would expect, increasing n, for the same h_0, causes a greater volume of sediments that are eroded from the bed (see, e.g., tests A1 to A3). The same occurs by keeping a constant rotational speed and reducing h_0.

From the analysis of Table 3, it is evident that the volume of the eroded sediments is balanced by the volume of the deposited sediments. The relative error ε is calculated as reported in equation (11):

$$\varepsilon = \frac{V_e - V_d}{V_e} \cdot 100 \ (\%), \quad (11)$$

and is on average equal to 2.6%, with a maximum value for test A1 (about 6.7%) and a minimum for test A2 (0.49%). This means that almost all the eroded sediments are deposited in the neighbourhood of the scour hole and, thus, the area affected by the presence of the propeller is a well-defined and confined zone.

The dimensionless eroded sediment volume (V_e/D_p^3) was plotted as a function of h_0/D_p and F_0, producing the contour graph shown in Fig. 15. Thus, knowing the position of the propeller with respect to the bed surface and its efflux velocity, it is possible to determine the respective volume of sediments eroded by the jet. At the same time, the eroded volume can be expressed as a function of the geometric characteristics of the scour hole, that are the maximum scour depth, the maximum scour width and the maximum length along the centreline, according to the following dimensionless relationships [equations (12-14)]:

$$\frac{V_e}{D_p^3} = 18.19 \left(\frac{d_s}{D_p} \right)^{2.26} \quad (12)$$

$$\frac{V_e}{D_p^3} = 0.22\left(\frac{b_s}{D_p}\right)^{2.60} \tag{13}$$

$$\frac{V_e}{D_p^3} = 0.05\left(\frac{l_{sc}}{D_p}\right)^{2.93} \tag{14}$$

for which R^2 is equal to 0.99, 0.99 and 0.96, respectively. Hence, using [equations (12-14)] and the abacus depicted in Fig. 16, one can derive all the geometrical characteristics of the scour hole if at least one of the quantity is known. For example, if the maximum scour depth induced by a ship propeller having a diameter of 0.1 m is equal to 0.1 m ($d_s/D_p = 1$), using Eq. (12) it is possible to obtain the corresponding value of V_e/D_p^3 (that is 18.2; therefore, $V_e = 0.018$ m^3). Consequently, the values of b_s/D_p and l_{sc}/D_p can be deduced from Eqs. (13) and (14), that are 5.42 and 7.48, respectively, which correspond to $b_s = 0.54$ m and $l_{sc} = 0.75$ m.

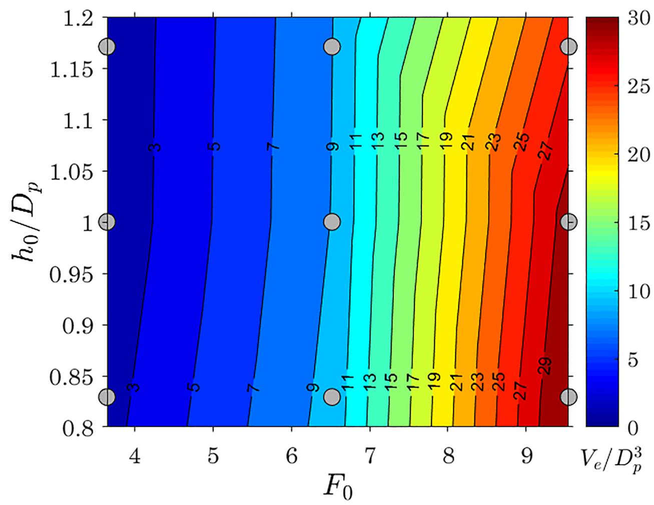

Figure 15 - Contour graph of the dimensionless eroded sediment volume (V_e/D_p^3) versus the dimensionless submergence depth (h_0/D_p) of the propeller and the Froude number (F_0).

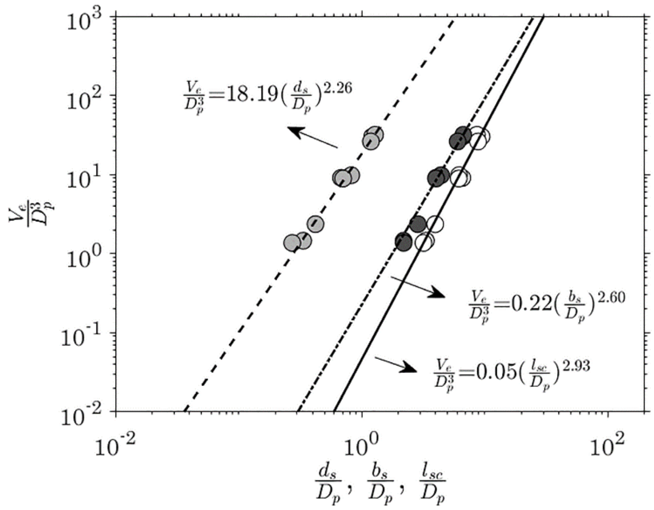

Figure 16 - Abacus of the geometrical characteristics of the scour hole induced by a rotating ship propeller.

5. Conclusions

This study examines the effects induced by a rotating ship propeller in different conditions of submergence depth and rotational speed, considering an unconfined jet.

Nine laboratory tests were performed and were characterized by densimetric Froude numbers that encompasses values typical of that encountered in many prototype situations (Hamill et al., 1999). The obtained results can be applied to full-scale propellers without significant scale effects related to the lower propeller Reynolds number (Wei and Chiew, 2017; Tan and Yüksel, 2018).

The temporal development of the scour profile along the centreline was measured by using an ADV during the scouring process, showing that the effect produced by the propeller consists in a small scour hole directly beneath the propeller and a main scour hole that expands downstream of it and creates a sediment mound that moves to downstream and enlarges gradually. The extension of these regions depends on the rotational speed of the propeller (for n = 270 rpm the small scour hole does not occur, whereas increasing n both the scour holes become wider and longer). It was also demonstrated that the scour profiles can be considered affine in time. The affinity is also preserved for the deposition mound in the last phase of the scouring process.

The creation of a high-resolution DEM, representing the bed surface affected by the propeller jet, allowed the investigation of the geometrical characteristics of the scour hole and of the deposition mound. Hence, the relationships between all these variables were analysed, providing useful equations, graphs and an abacus for the prediction of the effects induced by the propeller as a function of the submergence depth and of the Froude number.

Analysing the 3D characteristics of the scour hole in detail, it was demonstrated that the general hypothesis found in the literature that considers the scour hole symmetrical respect to the propeller longitudinal axis is not verified. In fact, the jet produced is essentially a swirling jet that, following the direction of the rotation, causes a deeper scour hole on one side and a higher deposition mound on the other side of the propeller. Thus, the maximum scour depth, as well as the maximum deposit height, does not necessarily occur at the centreline because of this swirling effect. The present study showed that only with a comprehensive and detailed analysis of the 3D characteristics of the scour hole it is possible to capture such a particular phenomenon. This was possible thanks to the technological advancement of laboratory instrumentation in the hydraulic field, which allows a better investigation of hydraulic phenomena (like scouring induced by a propeller) with respect to previous studies (Hager and Boes, 2014).

Thus, this paper provides several aspects that were not analysed in previous literature studies, filling the gap concerning the estimation of the eroded and deposited sediment volumes. The capability to predict such sediment volumes produced by rotating ship propellers is extremely important for the management of harbour basins, especially in terms of costs related to repair works (e.g., deposit dredging and filling operations). However, it should be pointed out that the sediment volumes (both eroded and deposited), as well as the other characteristic dimensions, were determined at the equilibrium condition, owing to the instruments setup used in this study, which, albeit innovative in this field, did not allow their underwater usage during the experiments. This could be considered as a limitation for the present study, but at the same time is a benchmark for further studies devoted to the monitoring of the time evolution of the eroded and deposited volumes by using new technologies (e.g., underwater drones).

At the same time, additional work in the future is required to take into account other variables that may affect the scouring phenomenon (e.g., propeller diameter, number of propellers, number of blades, water depth), as well as the median grain size of the bed material to study the effect of sediment resuspension induced by a ship propeller jet. This is a crucial aspect from the viewpoint of the water quality in a harbour basin, since contaminated materials usually associated to the finest fraction of sediments are recognized as a critical element for the aquatic ecosystem, requiring careful evaluation for the potential remediation of coastal areas. Another potential development of the present research work may be represented by the investigation of the effect induced by the propeller wake of a moving ship on the scouring formation.

However, it is important to highlight that experimental tests conducted on a physical model are not scaled-down versions of a particular prototype; they should be seen as tests for investigating a specific phenomenon, which in this case are the scouring and deposition processes induced by the rotation of a propeller near the seabed. The influence of scale effects must be further examined by running numerical tests at different scales to understand exhaustively the prototype situation, since the same tests performed in laboratory may require the use of always larger physical models up to the 1:1 scale.

Acknowledgements: This work was supported by the "SisTemi di rApid mapping e contRollo del Territorio costiero e marino (START)" Project (Regione Puglia, FSC 2007-2013, "Cluster Tecnologici Regionali" - Code 0POYPE3) and by the "Eco-Smart Breakwater" Project (Regione Puglia, FSC 2007-2013, "Cluster Tecnologici Regionali" - Code C6LU5I7).

References

Abramowicz-Gerigk, T. (2010). Distribution of flow velocity generated by propellers of twin propeller vessel. *Scientific Journals of the Maritime Academy of Szczecin*, 20(92), 5–12.

Bergh, H., & Magnussen, N. (1987). Propeller erosion and protection methods used in ferry terminals in the port of Stockholm. *Bulletin of the Permanent International Association of Navigation Congresses* (PIANC), 58, 112–120.

Blaauw, H. G., & Van de Kaa, E. J. (1978). *Erosion of Bottom and Sloping Banks caused by the Screw race of Maneuvering Ships*. Delft Hydraulics laboratory, Netherlands (No. 202). Report.

Chiew, Y. M., & Lim, S. Y. (1996). Local scour by a deeply submerged horizontal circular jet. *Journal of Hydraulic Engineering*, 122(9), 529–532.

Cihan, K., Ozan, A. Y., & Yüksel, Y. (2012). The effect of slope angle on propeller jet erosion near quays. Proceedings of the ICE–*Maritime Engineering*, 165(2), 81–92.

Froehlich, D. C., & Shea, C. C. (2000). Screwed-up riprap: Sizing rock linings to resist ship propeller-jets. In *Building Partnerships* (1–9).

Hager, W. H., & Boes, R. M. (2014). Hydraulic structures: a positive outlook into the future. *Journal of Hydraulic Research*, 52(3), 299–310.

Hamill, G. (1987). *Characteristics of the screw wash of a manoeuvring ship and the resulting bed scour*. Doctoral dissertation. Queen's University of Belfast.

Hamill, G. A., Johnston, H. T., & Stewart, D. P. (1999). Propeller wash scour near quay walls. *Journal of Waterway, Port, Coastal, and Ocean Engineering*, 125(4), 170–175.

Hamill, G. A., & Kee, C. (2016). Predicting axial velocity profiles within a diffusing marine propeller jet. *Ocean Engineering*, 124, 104–112.

Hamill, G., Kee, C., & Ryan, D. (2015). Three-dimension efflux velocity characteristics of marine propeller jets. Proceedings of the *ICE–Maritime Engineering*, 168(2), 62–75.

Hashmi, H. N. (1995). *Erosion of a granular bed at a quay wall by a ship's screw wash*. Doctoral dissertation. Queen's University of Belfast.

Hawkswood, M., Evans, G., & Hawkswood, G. (2013). Berth scour protection for fest ferry jets. In: *ICE Marine Structure and Breakwaters Conference, Edinburg, England*.

Hong, J. H., Chiew, Y. M., & Cheng, N. S. (2013). Scour caused by a propeller jet. *Journal of Hydraulic Engineering*, 139(9), 1003–1012.

Hong, J. H., Chiew, Y. M., Hsieh, S. C., Cheng, N. S., & Yeh, P. H. (2015). Propeller Jet–Induced Suspended-Sediment Concentration. *Journal of Hydraulic Engineering*, 142(4), 04015064.

Ji, S., Ouahsine, A., Smaoui, H., & Sergent, P. (2013). 3D Numerical Modeling of Sediment Resuspension Induced by the Compounding Effects of Ship-Generated Waves and the Ship Propeller. *Journal of Engineering Mechanics*, 140(6), 04014034.

Kelly, C. A., Ayoko, G. A., Brown, R. J., & Swaroop, C. R. (2005). Underwater emissions from a two-stroke outboard engine: a comparison between an EAL and an equivalent mineral lubricant. *Materials & design*, 26(7), 609-617.

Lam, W. H., Hamill, G., Robinson, D., & Raghunathan, S. (2010). Observations of the initial 3D flow from a ship's propeller. *Ocean Engineering*, 37(14–15), 1380–1388.

Lam, W. H., Hamill, G., Robinson, D., Raghunathan, S., & Song, Y. (2012). Analysis of the 3D zone of flow establishment from a ship's propeller. KSCE *Journal of Civil Engineering*, 16(4), 465–477.

Lam, W. H., Hamill, G. A., Song, Y. C., Robinson, D. J., & Raghunathan, S. (2011). A review of the equations used to predict the velocity distribution within a ship's propeller jet. *Ocean Engineering*, 38(1), 1–10.

Mujal-Colilles, A., Gironella, X., Sanchez-Arcilla, A., Puig Polo, C., & Garcia-Leon, M. (2017). Erosion caused by propeller jets in a low energy harbour basin. *Journal of Hydraulic Research*, 55(1), 121–128.

Ozan, A. Y., Cihan, K., & Yüksel, Y. (2012). Propeller induced scour around the pile type berth structures. *Applied Ocean Research*, 38, 16–22.

Ozan, A. Y., & Yüksel, Y. (2010). Simulation of a 3D submerged jet flow around a pile. *Ocean Engineering*, 37(8–9), 819–832.

PIANC (Permanent International Association of Navigation Congresses). (2015). *Guidelines for protecting berthing structures from scour caused by ships*. Rep. No. 180.

Qurrain, R. M. M. (1994). *Influence of the sea bed and berth geometry on the hydrodynamics of the wash from a ship's propeller*. Doctoral dissertation. Queen's University of Belfast.

Ryan, D. (2002). *Methods for determining propeller wash induced scour in harbours*. Doctoral dissertation. Queen's University of Belfast.

Schokking, L. A., Janssen, P. C., & Verhagen, H. J. (2002). Bowthruster-induced damage. *Bulletin of the Permanent International Association of Navigation Congresses* (PIANC), 114, 53–63.

Smith, E.R., D'Alessandro, F., Tomasicchio, G.R., Gailani, J.Z. (2017). Nearshore placement of a sand dredged mound. *Coastal Engineering*, 126, 1–10.

Stewart, D. P. J. (1992). *Characteristics of a ship's screw wash and the influence of quay wall proximity*. Doctoral dissertation. Queen's University of Belfast.

Sumer, B. M., & Fredsøe, J. (2002). *The mechanics of scour in the marine environment*, Advanced Series on Ocean Engineering, 17.

Tan, R. İ., & Yüksel, Y. (2018). Seabed scour induced by a propeller jet. *Ocean Engineering*, 160, 132–142.

Verhey, H. (1983). The stability of bottom and banks subjected to the velocities in the propeller jet behind ships. In: *International Harbour Congress, 8th, Antwerp, Belgium*.

Wei, M., & Chiew, Y. M. (2017). Influence of toe clearance on propeller scour around an open-type quay. *Journal of Hydraulic Engineering*, 143(7), 04017012.

Wei, M., & Chiew, Y. M. (2018). Characteristics of propeller jet flow within developing scour holes around an open quay. *Journal of Hydraulic Engineering*, 144(7), 04018040.

Wei, M., Chiew, Y. M., & Guan, D. (2018). Temporal Development of Propeller Scour around a Sloping Bank. *Journal of Waterway, Port, Coastal, and Ocean Engineering*, 144(5), 06018005.

Whitehouse, R. (1998). *Scour at marine structures: A manual for practical applications*. Thomas Telford.

Yeh, P. H., Chang, K. A., Henriksen, J., Edge, B., Chang, P., Silver, A., & Vargas, A. (2009). Large-scale laboratory experiment on erosion of sand beds by moving circular vertical jets. *Ocean Engineering*, 36(3–4), 248–255.

Yew, W. T., Hashim, R., & Ng, K. C. (2017). Experimental investigation on axial velocity distribution for ship's twin-propeller jets. *Journal of the Chinese Institute of Engineers*, 40(3), 191–199.

Yüksel, A., C¸elikoğlu, Y., C¸evik, E., & Yüksel, Y. (2005). Jet scour around vertical piles and pile groups. *Ocean Engineering*, 32(3–4), 349–362.

Yüksel, Y., Tan, R. I., & C¸elikoğlu, Y. (2018). Propeller jet flow scour around a pile structure. *Applied Ocean Research*, 79, 160–172.